Polarization distribution in ceramic-polymer nanocomposites

Peter Bloss[a] and Aimé S. DeReggi
Polymers Division, Bldg. 224/Rm. B320, National Institute of Standards and Technology, Gaithersburg, Maryland 20899

Hans-Jürgen Gläsel, Eberhard Hartmann,[b] and Dietmar Hirsch
Institute of Surface Modification (IOM), Permoserstraße 15, D-04318 Leipzig, Germany

Hartmut Schäfer
HF-NMR Facility, NSR Center, University of Nijmegen, Toernooiveld 1, NL-6525 Nijmegen, Netherlands

(Received 15 March 1999; accepted for publication 24 May 1999)

We report pyroelectric responsivity versus depth profiles in nanocomposites of powdered barium titanate and tripropylene glycol diacrylate obtained by using the thermal pulse (TP) method. The cerámic nanopowder (mean particle size 270 nm) was prepared by combined solid-state polymerization and pyrolysis of a metallo-organic precursor. Films of powder/monomer dispersion (thickness ~30 μm) were cured by irradiation with an electron beam (energy 140 keV, dose 80 kGy). The observation of a TP response after electron beam curing (EBC) indicates the appearance of a poling electric field as an effect of the EBC. The polarization depth profiles were studied for different filler contents. The composites show potential promise for piezo and pyroelectric sensors applications and for charge storage in microelectronics. © *1999 American Institute of Physics.* [S0021-8979(99)03417-9]

I. INTRODUCTION

Polymer-ceramic composites can combine advantageous properties of both the polymer (such as flexibility, easy processing) and the ceramic (high dielectric permittivity, high piezo and pyroelectric activity).[1,2] They are under extensive study as technologically promising, integrated-capacitor thin film materials offering both high dielectric permittivity and low loss.[3] The novel processing of such films has often led to empirically adopted processing details before their effects on electrical, mechanical, and thermal properties were fully understood. Electron beam irradiation used to cure polymeric binders may, for example, create internal poling electric fields[4] that depend on the electron energy and dose as well as on the relative concentrations of the components and the ratio of their dielectric constants. The electric fields induced during the electron beam curing (EBC) may lead to a partial poling of the nanocomposite with a polarization distribution across the thickness distinct from the more uniform one expected in the same material poled by an external constant electric field.

The attainment of a homogeneous ceramic-powder dispersion calls for particles that are as small as possible. However, the particle size cannot be made arbitrarily small if the ferroelectricity is to be maintained, since ferroelectricity is a cooperative phenomenon. A loss of ferroelectric behavior has been reported at a reduced dimension.[5] In addition, a decrease of the correlation length below the geometric length has been observed and attributed to lattice defects.[6] Consequently, for optimizing ferroelectric ceramic/polymer nanocomposites, there is an urgent need for well characterized ferroelectric powders combining intermediate particle size with low defect concentration.

Our preparation of ferroelectric ceramic/polymer nanocomposites is based on combined polymerization and pyrolysis of metallo-organic precursors as a novel particle preparation method[7] and the EBC of thin dispersion films of ferroelectric barium titanate ($BaTiO_3$) nanopowders in monomeric acrylates. We present an investigation of poling and switching behavior of the composites, which contributes new information in the growing field of thin-film radiation-processing applications.

II. PREPARATION OF THE NANOCOMPOSITE

A. Preparation and characterization of the $BaTiO_3$ particles

Different ways of preparing nanocrystalline $BaTiO_3$ particles are known, e.g., pyrolysis of peroxides,[8] sol-gel processes,[9,10] gas-condensation processes,[11] and chemical precipitation from solution.[12] Our preparation route of $BaTiO_3$ nanopowders is described here briefly by four reactions (details are given elsewhere):[7] In a first step, barium titanium methacrylate is obtained as a monomeric metallo-organic precursor from metallic barium, titanium IV isopropylate and methacrylic acid in boiling methanol. Then, the solid-phase polymerization and the concomitant pyrolysis proceed simultaneously at temperatures above 200 °C. A subsequent nucleation and growth of the $BaTiO_3$ particles take place at reaction temperatures above 600 °C. The resulting particle size is determined by the reaction temperature, reaction atmosphere, and the annealing time at the reaction temperature under the reaction atmosphere, e.g., we have ob-

[a]Permanent address: Kunststoff-Zentrum in Leipzig gemeinnützige Gesellschaft mbH Erich-Zeigner-Allee 44, D-04229 Leipzig, Germany.
[b]Author to whom correspondence should be addressed; electronic mail: hartmann@rz.uni-leipzig.de

tained 10 nm particles at 600 °C under a N_2 atmosphere for an annealing time of two days and 1.3 μm particles under an O_2 atmosphere for two days at 1350 °C. Our 270 nm particles were obtained at 1300 °C under N_2. The ability to adjust the particle size by just choosing the appropriate reaction temperature and atmosphere is the salient advantageous feature of our preparation route.

The average size of the particles, d, was determined by x-ray diffraction. The effects of the lattice distortions were taken into account according to the method of Warren and Averbach.[13,14] The standard uncertainty in d for our particles ($d=270$ nm) was ± 20 nm.

$BaTiO_3$ is a displacive-type ferroelectric with a paraelectric-ferroelectric transition at a Curie temperature T_c of 120 °C as detected for example by vibrational spectroscopy.[15] An earlier study of $BaTiO_3$ bulk systems[7] found that some characteristic Raman features appear in the wavenumber range from 50 to 800 cm^{-1}. Particularly the intensity of the "tetragonal" vibration band at 309 cm^{-1} revealed a transition behavior, where smearing effects increase with the decreasing particle size, thus confirming a decrease of ferroelectric order at small dimensions. However, the corresponding results for the 270 nm particles testified to the existence of ferroelectric properties, with presumed spontaneous polarization. Thus, the poling and switching behavior of the latter represents a relevant subject in the present investigations.

B. EBC of the nanocomposite

At first, the $BaTiO_3$ nanopowder was dispersed in the tripropylene glycol diacrylate (TPGDA) monomer (Cray Valley,[16] p.A. grade) with the aid of a planetary ball mill under soft grinding conditions (low rotation frequency, small number of small milling balls, 5 min milling time). Then, by using the doctor-blade coater (type SIMEX AF-3),[16] thin films (~50-mm-thick) of different particle/monomer dispersions (concentration w/w) were produced on glass substrates. The films were cured by using a previously described low-energy electron accelerator built at the Institute of Surface Modification, Leipzig, Germany as described earlier.[17] The curing energy and dose in these investigations were 140 keV and 80 kGy respectively. The surface through which the electron beam entered the sample is labeled "front" (located at $z=0$, where z is the depth coordinate), and the opposite surface in contact with the substrate is labeled "rear" (at $z=L$, where L is the thickness of the composite foil). After a 10 h immersion in a water bath, the composite foils could be readily detached from the substrate. The composites proved to be flexible up to a $BaTiO_3$ mass fraction of 50%.

The thickness of the films was measured with a mechanical thickness gauge at ten positions across the sample diameter. The values for the thickness are mean values (standard deviation ~2 μm).

C. Scanning electron microscopy

Scanning electron microscopy (SEM) images were obtained at 30 keV using a JEOL JSM-6600 instrument.[16] Electron-excited x-ray spectra (EDX) were obtained using a RONTEC M3 EDX imaging system[16] attached to the SEM. Sample cross sections suitable for imaging were obtained by cryobreaking in liquid N_2. In order to prevent secondary x-ray excitation in the EDX measurements the samples were coated with a 10-nm-thick carbon layer using a LEYBOLD Z 400 sputter deposition coater.[16] This layer makes only a small contribution to the CK_α line (less than 10%).

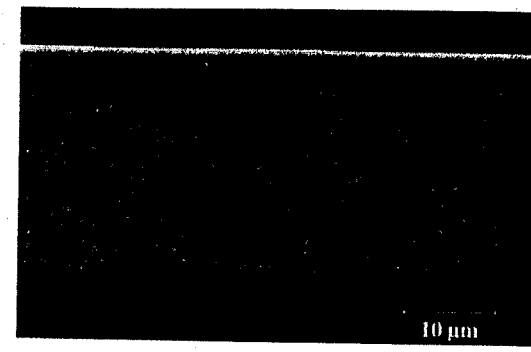

FIG. 1. SEM image of a face broken of a composite sample (thickness 28 μm, average particle concentration 50%, mean particle size 270 nm).

A SEM image for a composition of 40 wt. % $BaTiO_3$ and 270 nm mean particle size is shown in Fig. 1. The bright shining edge near the top of the figure (a SEM geometry effect) locates the front surface. The contrast between the $BaTiO_3$ particles and the polymer matrix is due to the higher secondary electron emission of the particles. At the lower edge (the rear surface) the density and size of the $BaTiO_3$ particles are obviously increased as compared with the upper face region near the front surface. This enrichment near the lower rear surface indicates a sedimentation process occurring in the particle/monomer dispersion prior to the EBC.

EDX spectra were taken from regions of the cross section near the front and rear surfaces. For clarity, an appropriate upward shift (by 5×10^3 counts) of the "front spectrum" has been introduced in Fig. 2. In the EDX measurements, the electron beam was scanned over areas of about 30 μm^2 so that at the probing depth of about 1.7 μm, the analyzed volumes were about 50 μm^3. From the volume-averaged Ba and Ti x-ray line intensities a rear to front $BaTiO_3$ concentration ratio of about six was estimated. Some

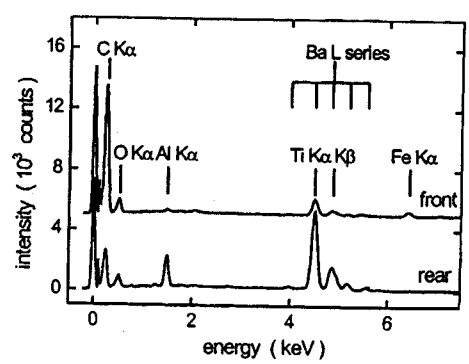

FIG. 2. EDX spectra taken from face regions near front and rear surfaces, respectively.

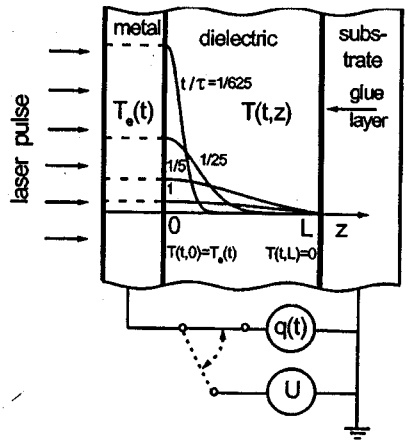

FIG. 3. Schematic for TP measurement.

concomitant lines (AlK_α,FeK_α) are due to secondary emissions from the deeper lying sample holder.

III. THERMAL PULSE INVESTIGATIONS

A. Thermal pulse–response description

1. Model for sample and basic equations

The model for the thermal pulse (TP) experiments is shown in Fig. 3. The dielectric film, with metal (vacuum deposited Al) electrodes of thickness $L_e \approx 100$ nm on both sides, is glued to a copper block with an electrically conductive glue. The TP response, $q(t)$, of the sample is a convolution of the pyroelectric responsivity, $G(z)$, and the TP-induced strain proportional to the TP-induced temperature change $T(t,z)$. The TP equation is[18]

$$q(t)=\int_0^L L(t,z)G(z)dz, \tag{1}$$

where t is the time coordinate and z is the depth coordinate measured from the incident surface. In general, $G(z)$ contains contributions from the dipole polarization with the pyroelectric coefficient, $g(z)$, and from the internal electric field, $E(z)$, produced by space charge according to[18]

$$G(z)=-\frac{A}{L}g(z)+\alpha_C CE(z), \tag{2}$$

where A is the electrode area and $\alpha_C C=\partial C/\partial T$ is the temperature coefficient of the sample capacitance C.

The kernel $T(t,z)$ is the solution of the one-dimensional heat conduction equation for an electroded planar sample with one surface contacting an ideal heat sink. The appropriate boundary conditions are

$$-\kappa\frac{\partial T}{\partial z}+\rho_e c_e L_e\frac{\partial T}{\partial t}=J_0\delta(t) \tag{3}$$

at the TP-incident side and

$$T=0 \tag{4}$$

at the opposite, thermally contacted, side of the sample. The TP associated with the infinitesimally short laser pulse is $J_0\delta(t)$, in which $\delta(t)$ is the Dirac delta function. The symbol κ is the heat conductivity of the dielectric, $\rho_e c_e L_e$ is the thermal mass (per unit area) of the electrode, where ρ_e is its mass density and c_e is its specific heat. The solution, $T(t,z)$, may be obtained by using Laplace transformation[19] and is

$$T(t,z)=T_\infty 2\sum_{k=0}^{\infty}\frac{\sin\left[x_k\left(1-\frac{z}{L}\right)\right]}{(1+r+r^2x_k^2)\sin(x_k)}\exp\left(-x_k^2\frac{t}{2\tau}\right), \tag{5}$$

where $T_\infty=J_0L/\kappa$ is the $t\to\infty$ asymptotic value of $T(t,z)$ for the hypothetical case of an isolated sample with negligible electrode thermal mass. The parameter r given by

$$r=\frac{\rho_e c_e L_e}{\rho c L}=\frac{\kappa_e}{\kappa}\frac{D}{D_e}\frac{L_e}{L} \tag{6}$$

expresses the ratio of the thermal mass of the electrode to the thermal mass of the dielectric. In Eq. (6), the well known relation $\rho c=\kappa/D$, where κ is the thermal conductivity, D is the thermal diffusivity, and ρc is the specific heat per unit volume, was used. The parameter $\tau=L^2/(2D)$ is the thermal transit time for the dielectric. The roots x_k have to be determined numerically from the equation $\cos(x)-rx\cos(x)=0$, where $k\pi\leqslant x_k\leqslant(k+1/2)\pi$.[20]

The temperature profiles may be seen in Fig. 3 for different reduced times, $t/\tau=(1/625,1/25,1/5,1)$. It is assumed that the temperature across the metal electrode is uniform, and the thermal resistance between the electrode and the dielectric is zero [Eq. (3)]. These assumptions make sense because the thermal transit time for a 100-nm-thick aluminum electrode (where $D_e=9.8\times10^{-5}$ m^2/s)[21] is $\tau_e=L_e^2/(2D_e)$ $\sim$50 ps, which is much smaller than the time resolution of our equipment (the minimum time used for deconvolution is 100 ns, Sec. III B).

For samples with a spatially uniform $G(z)$ [Eq. (1)], namely uniformly poled and/or charge-free samples, $q(t)$ is proportional to the mean temperature $\langle T\rangle$

$$\langle T\rangle=\frac{1}{L}\int_0^L T(t,z)dz. \tag{7}$$

The reduced mean temperature is defined by $\langle T_{\rm red}\rangle=\langle T\rangle/T_\infty$, where T_∞ is the limit of $T(t,z)$ as t goes to infinity.

2. Simulations

Simple simulations for $\langle T\rangle$ were performed to show the shape of the TP responses to be expected from charge-free and/or homogeneously poled samples in the thickness range of our samples. The thermal properties[22] of the dielectric TPGDA were $\kappa=0.19$ W/(m×K), $\rho=1190$ kg/m^3, and $c=1470$ J/(kg×K), yielding the thermal diffusivity $D=1.09\times10^{-7}$ m^2/s. The ($L_e=100$-nm-thick) electrodes were assumed to have bulk-Al values for $\kappa_e=237$ W/(m×K) and $D_e=9.8\times10^{-5}$ m^2/s taken from a handbook.[21]

Figure 4 shows $\langle T_{\rm red}\rangle$ vs t for thicknesses $L=(10,30,50,70)$ μm, yielding $r\times10^3=13.9,4.62,2.77,1.98$, respectively. The penetration depth

$$\delta=\sqrt{2Dt} \tag{8}$$

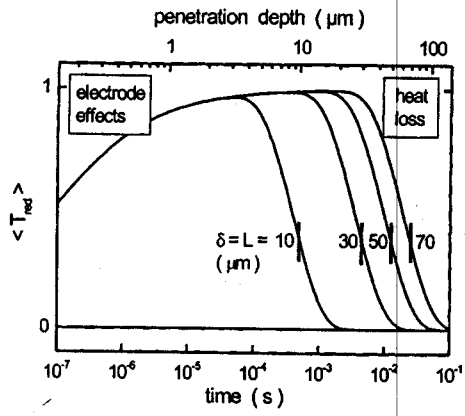

FIG. 4. Reduced mean temperature, $\langle T_{red}\rangle$, as a function of time, t, for different sample thicknesses $L=(10,30,50,70)$ μm. The upper scale shows the penetration depth, $\delta=\sqrt{(2Dt)}$, where D is the thermal diffusivity of the dielectric. The decay due to heat loss appears around $t\sim\tau=L^2/(2D)$ as marked by a small perpendicular line. The gradual increase of $\langle T_{red}\rangle$ with time at times $t\ll\tau$ is due to heat storage in the incident electrode at the TP side. Thermal parameters are given in Sec. III A 2.

is plotted in the upper x axis. The small perpendicular lines on the curves mark the time $t=\tau$, when $\delta=L$. The decay of the curves around $t\sim\tau$ is due to the heat loss to the substrate. The gradual increase of $\langle T_{red}\rangle$ with increasing t, for $t<\tau$ is due to heat storage effects of the electrode. Further details may be found elsewhere.[20]

Figure 5 shows $\langle T_{red}\rangle$ vs t for $L=70$ μm. The two curves around the zero baseline are deviations which are calculated as follows: $\Delta(-20\%)=\langle T_{red}\rangle(D)-\langle T_{red}\rangle(0.8\times D)$ and $\Delta(+20\%)=\langle T_{red}\rangle(D)-\langle T_{red}\rangle(1.2\times D)$. The deviations from the zero baseline of these curves show the strongly varying influence of D on $\langle T_{red}\rangle$ within the time range of the measurement. The D is more strongly weighted near the dielectric/substrate interface than near the TP-incident side.

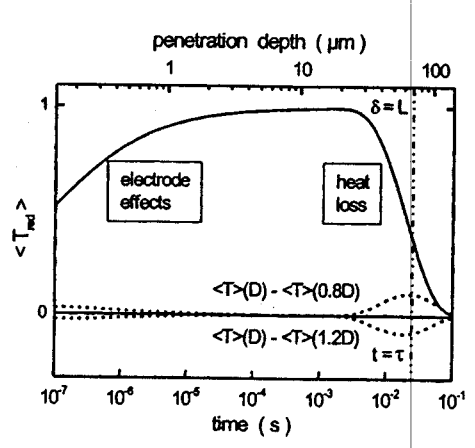

FIG. 5. Reduced mean temperature, $\langle T_{red}\rangle$, as a function of time. The curves close to the abscissa were determined as follows: $\Delta(-20\%)=\langle T_{red}\rangle(D)-\langle T_{red}\rangle(0.8\times D)$ and $\Delta(+20\%)=\langle T_{red}\rangle(D)-\langle T_{red}\rangle(1.2\times D)$. The deviation from the zero baseline is a measure of the weighting of deviations of D on $\langle T_{red}\rangle$. The thickness was 70 μm and the thermal parameters are given in Sec. III A 2.

3. Deconvolution of the TP equation

The TP equation [Eq. (1)] was deconvolved by using Tikhonov regularization[23] with a self-consistently determined regularization parameter.[24,25] The spatial function $G(z)$ was determined for a number of grid points, z_n (where $n=1,...,N$ with N as the number of grid points), which are following a power law according to

$$z_n=\left(\frac{n-1}{N-1}\right)^{\beta}\times L. \tag{9}$$

The number of grid points was chosen between 31 and 51 so that the exponent β was $\approx$0.5 (diffusion adapted). For the deconvolution ~2000 measuring points were used. The residuals d_m defining the quality of the fit for measuring points t_m, are

$$d_m=q^{\sigma}(t_m)-q(t_m,E), \tag{10}$$

where $q^{\sigma}(t_m)$ is the measured response with a noise amplitude σ and $q(t_m,E)$ is the recalculated response. The thermal diffusivity (D) of the sample was treated as a z-independent variable parameter. Further details about our procedure may be found elsewhere.[20,26,27]

B. Experimental results

1. TP procedure

One surface of a sample was Ag-epoxy bonded to a heat sinking copper block, leaving only the opposite surface as the external surface. Two similar samples were used to make the front and back surfaces available separately as TP-incident surfaces. All TP experiments were performed at room temperature (24 °C) with the sample under short-circuit conditions.

A glass plate beam splitter reflected a small part of the incident light and diverted it into a fast photodiode which allowed for the simultaneous recording of the light pulse temporal profile and the TP response. The Gaussian width of the laser pulse was 70 ns with a standard deviation of about 1 ns determined from a fit of 80 points 5 ns apart. The peak of the laser pulse was used as the origin ($t=0$) of all TP responses.

2. Samples without additional poling

Radiation-poled samples were first investigated without additional poling by an external applied voltage. Figures 6 and 7 show measured complementary TP responses versus time, $q_0(t)$, with the TP applied to the electrode at $z=0$, and $q_L(t)$ with the TP applied to the electrode at $z=L$. The TP measurements were carried out about two months after the EBC. The tail of the TP is shown in the bottom left and middle left portion of Figs. 6 and 7, respectively.

Figure 6 shows the TP responses of the type $q_0(t)$ for a 73-μm-thick polymer (electron beam cured TPGDA) film, a 68-μm-thick composite film with 20 wt.% $BaTiO_3$, a 62-μm-thick composite film with 40 wt.% $BaTiO_3$, and a 18-μm-thick composite film with 70 wt.% $BaTiO_3$. The $q_0(t)$ with the shortest duration in Fig. 6 belongs to the thinnest sample (70 wt.% $BaTiO_3$, 18μm). This is as expected from the L^2 dependence of the thermal transit time $\tau=L^2/(2D)$.

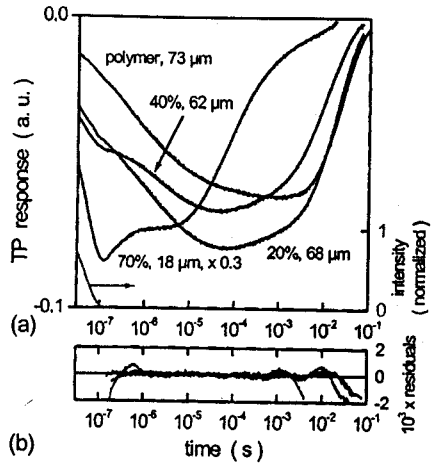

FIG. 6. (a) TP responses, $q_0(t)$, obtained when the TP was applied to front side (where the curing electron beam entered the sample). Thicknesses of polymer sample and of 20, 40, and 70 wt. % $BaTiO_3$ samples are respectively (73, 68, 62 and 18) μm. Tail of the TP at bottom left. 70% curve multiplied by 0.3. (b) Residuals of deconvolution (note smallness of residuals considering the magnified residuals scale).

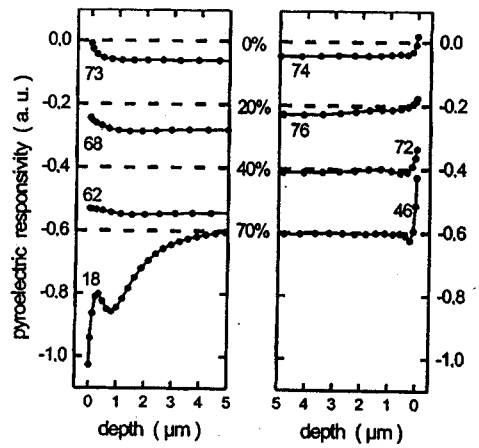

FIG. 8. Pyroelectric responsivity distribution, $G(z)$, in the near front and rear side region obtained from the TP responses shown in Figs. 6 and 7, respectively. The abscissas (dashed lines) are shifted (−0.2), (−0.4), and (−0.6) units for the curves for 20, 40, and 70 wt. % $BaTiO_3$ particle concentration, respectively.

Figure 7 shows the TP responses of the type $q_L(t)$ for a 74-μm-thick polymer film, a 76-μm-thick composite film with 20% $BaTiO_3$, a 72-μm-thick composite film with 40% $BaTiO_3$, and a 46-μm-thick composite film with 70 wt. % $BaTiO_3$.

The TP responses of these samples, indicate that the EBC process has produced a pyroelectric responsivity with a distribution $G(z)$. The $G(z)$ in the polymer is attributed to dipoles in the polymer presumed polar, but not necessarily ferroelectric. The $G(z)$ in the nanocomposites thus has both a ferroelectric part from the $BaTiO_3$ particles in addition to a part from the TPGDA. The responses $q_L(t)$ (Fig. 7) have smaller amplitudes than $q_0(t)$, meaning that $G(z)$ near $z=L$ is smaller than that near $z=0$.

The similar shapes (apart from a trivial sign reversal due to the hookup) of the TP responses for the unfilled polymer, regardless of whether the EBC surface or the rear surface is thermally pulsed (Figs. 6 and 7) suggest, independently of the deconvolutions, that $G(z)$ in the unfilled polymer is nearly symmetric. The qualitative similarity of these shapes with the shape of $\langle T \rangle$ calculated for a homogeneous sample under a constant field indicate that the polarization induced in the neat polymer is uniform in a first approximation. A uniform polarization is consistent with the response of a polar, nonferroelectric material in a uniform field. This suggests that any charges deposited during the EBC process tend to remain concentrated near the surfaces. The responses for the $BaTiO_3$-filled samples are seen to deviate strongly from the response of the neat polymer. This may indicate simply an inhomogeneous distribution of particles. An alternative explanation based on space charge distortions of the poling field would imply extended charge distributions, which is markedly unlike the neat polymer results.

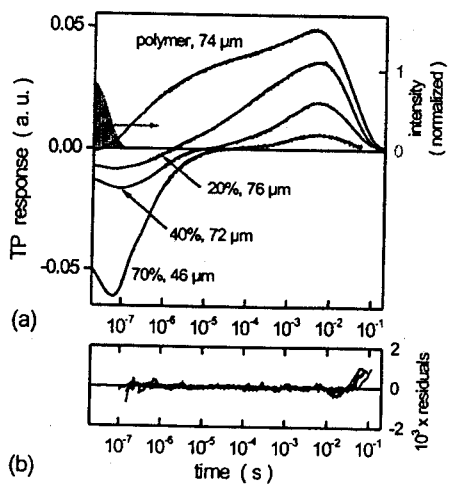

FIG. 7. Same as Fig. 6, but the rear side TP responses, $q_L(t)$, (side which was on the glass substrate during EBC). The thicknesses (in μm) are 74, 76, 72, and 46.

Figure 8 shows $G(z)$ in the near surface region obtained by deconvolving the $q_0(t)$ and $q_L(t)$ results in Figs. 6 and 7, respectively. The statistical error bars with a 68% confidence limit (omitted for clarity) have, at most, the same size as the symbols. These results confirm that the polymer is nearly homogeneously poled, whereas the composites show a more complex behavior. The evolution of $G(z)$ with an increasing $BaTiO_3$ content indicates increasing deviations of the polarization distribution from the uniform distribution of the polymer. For samples containing 70 wt. % $BaTiO_3$, the deviations include sharp features within shallow depths of both surfaces (negative for the front surface and positive for the rear surface), and a broad negative peak in the front half of the sample. The broad peak is assigned to ferroelectric polarization in the inhomogeneously dispersed ceramic particles. The shape of this broad peak is determined by both the ceramic particle concentration and the EBC-induced poling field. It is reasonable to expect that, at a high $BaTiO_3$ content, enough electrons were stopped in the rear half of the sample to reverse the poling field near the rear. This may account for the positive values of $G(z)$ towards the rear sur-

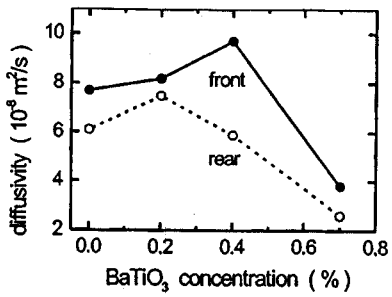

FIG. 9. Effective thermal diffusivities as a function of the $BaTiO_3$ particle concentration.

face along with the negative values of $G(z)$ towards the front surface. The rear-to-front ceramic particle density ratio of six revealed by EDX may be explained by an offsetting weakness of the EBC field in the thickness range where this field is reversed.

Figure 9 shows the values for the thermal diffusivity D (standard uncertainty is ~10%) versus the $BaTiO_3$ content. These values were determined by treating D as a z-independent fitting parameter. In case of a z dependence in D, this value becomes an effective value, influenced by the weighting effects of both the kernel $T(t,z)$ and the sample-dependent $G(z)$. The dependence of D on the $BaTiO_3$ content is then no longer simply interpretable.

The observed decrease in D for the $BaTiO_3$ contents higher than 20% was not expected, since the diffusivity of $BaTiO_3$ exceeds the corresponding value of the polymer by a factor of about 20, see e.g., in Ref. 28. A radiation-induced sample porosity may be the reason for this behavior. This possibility is now under investigation.

For constant $G(z)$,$q(t)$ is most strongly affected by D at long times meaning an effective value of D is more strongly determined by the thickness range near the sample/substrate interface (see discussion for Fig. 5 in Sec. III A 2). Since D of $BaTiO_3$ is bigger than D of the polymer, a bigger D indicates a higher $BaTiO_3$ content. Consequently, a bigger D obtained from $q_0(t)$ than D obtained from $q_L(t)$ indicates a

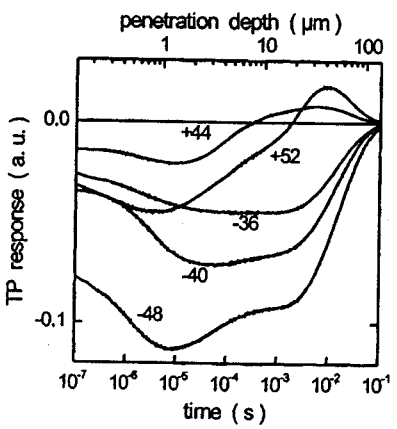

FIG. 10. Front side TP response for the sample with a 40 wt. % $BaTiO_3$ concentration and $L=62\,\mu$m. Numbers represent mean fields in V/μm, where the bias voltage is applied to the back side of the sample. Penetration depth is $\sqrt{(2Dt)}$ with $D=9.5\times10^{-8}$ m²/s.

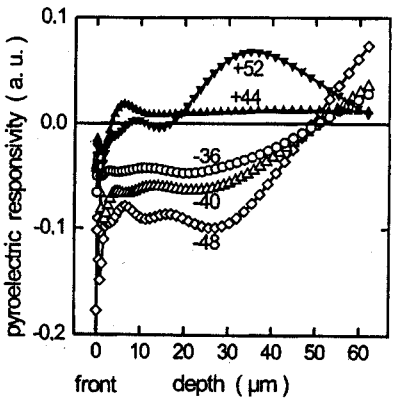

FIG. 11. Spatial distributions, $G(z)$, determined from the TP responses in Fig. 10. Open and solid symbols are for negative and positive voltages applied to the back side, respectively. Thickness is $L=62\,\mu$m.

higher $BaTiO_3$ particle content at the rear side (the side at the substrate during EBC). The conclusion from D is that the $BaTiO_3$ particles are more highly concentrated near the rear side as shown by the EDX results described in Sec. II C.

3. Samples with additional poling

The EBC-poled samples were additionally poled at room temperature under various applied voltages. Figure 10 shows the TP responses for the 40 wt. % $BaTiO_3$, $L=62$-μm-thick (front-side sample), for several voltages applied to the back electrode in the following order: (−36, −40, −48, +44, and +52) V/μm. The front electrode was grounded. Each voltage was applied for 2 h at room temperature. Afterwards the electrodes were shorted for 3 h and then the TP experiment was performed. The spatial distributions $G(z)$ obtained by the deconvolution of the responses in Fig. 10 are shown in Fig. 11. Figure 12 shows an expanded front surface region.

As expected, negative voltages produce electric polarization over most of the thickness in the same direction as the polarization already produced by the EBC process when the electron energy was high enough for the electron range to be comparable to L. The positive fields tend to reverse this polarization, the highest field (+52 V/μm) having switched the polarization over a large part of the sample.

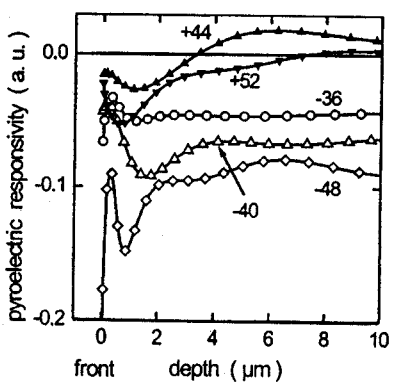

FIG. 12. Same as Fig. 11, but near front surface region expanded.

IV. CONCLUSION

This work shows conclusively that EBC produces rather complex internal field distributions with peak values large enough to partially pole the ferroelectric particles and the polymeric binder. An estimate of the peak magnitude of the EBC-induced fields of 50 V/μm may be made from the strength of the TP responses of the virgin samples or from the strength of the reverse external fields required to cancel the TP responses of the virgin samples. As we have seen, the inhomogeneity in the powder dispersion affects not only the polarization distribution but also the thermal properties distribution. The large disparity in diffusivity between the ceramic and polymer is clearly seen as a $BaTiO_3$-concentration-dependent effective diffusivity. This means that a more detailed numerical analysis of the TP results would need to take into account the diffusivity distribution.

ACKNOWLEDGMENTS

Valuable discussions with Dr. G. T. Davis, Dr. Wen-li Wu, Dr. C. Snyder, and Dr. J. Obrzut of NIST are gratefully acknowledged. One of the authors (P.B.) is grateful to NIST for financial support.

[1] K. Mazur, *Polymer-Ferroelectric Ceramic Composites, in: Ferroelectric Polymers*, edited by H. S. Nalwa (Marcel Dekker, New York, 1995).
[2] C. J. Dias and D. K. DasGupta, IEEE Trans. Dielectr. Electr. Insul. **3**, 706 (1996).
[3] H. J. Cho and H. J. Kim, Appl. Phys. Lett. **72**, 786 (1998).
[4] A. S. DeReggi, A. J. Bur, F. I. Mopsik, and C. Dick, Bull. Am. Phys. Soc. **23**, 294 (1983).
[5] W. L. Zhong, Y. G. Wang, P. L. Zhang, and B. D. Qu, Phys. Rev. B **50**, 698 (1994).
[6] S. Wada, T. Suzuki, and T. Noma, Jpn. J. Appl. Phys., Part 1 **34**, 5368 (1995).
[7] H.-J. Gläsel *et al.*, J. Mater. Sci. **34**, 2319 (1999).
[8] Y. L. Fang, W. K. Zhao, and R. H. Wang, Chem. J. Chines. Univ. **17**, 1685 (1996).
[9] L. A. Bursill, B. Jiang, and J. L. Peng, Ferroelectrics **191**, 489 (1997).
[10] M. C. Gust, N. D. Evans, and L. A. Momoda, J. Am. Ceram. Soc. **80**, 2828 (1997).
[11] S. P. Li, J. A. Eastman, and L. J. Thomson, Appl. Phys. Lett. **70**, 2244 (1997).
[12] R. W. Schwartz, Chem. Mater. **9**, 2325 (1997).
[13] B. E. Warren and B. L. Averbach, J. Appl. Phys. **21**, 595 (1950).
[14] B. E. Warren, Acta Crystallogr. **8**, 483 (1955).
[15] L. H. Robins, D. L. Kaiser, L. D. Rotter, and G. T. Stauf, Mater. Res. Soc. Symp. Proc. **341**, 315 (1994).
[16] The use of commercial names to identify the materials and equipment in no way implies endorsement or recommendation by NIST.
[17] R. Mehnert, P. Klenert, and E. Hartmann, Nucl. Instrum. Methods Phys. Res. B **68**, 73 (1992).
[18] G. F. Leal Ferreira and R. Gerhard-Multhaupt, Phys. Rev. B **42**, 7317 (1990).
[19] H. S. Carslaw and J. C. Jaeger, *Conduction of Heat in Solids*, 2nd ed. (Clarendon, Oxford, 1995).
[20] P. Bloss, A. S. DeReggi, and H. Schäfer, Phys. Rev. B (submitted).
[21] *Handbook of Chemistry and Physics*, 75th edited by D. R. Lide (CRC Press, Boca Raton, 1994).
[22] *Polymer Handbook*, 3rd ed., edited by J. Brandrup and E. H. Immergut (Wiley New York, 1989).
[23] A. N. Tikhonov and V. Y. Arsenin, *Solution of Ill-posed Problems* (Wiley, New York, 1977).
[24] J. Honerkamp and J. Weese, Continuum Mech. Thermodyn. **2**, 17 (1990).
[25] J. Weese, Comput. Phys. Commun. **69**, 99 (1992).
[26] P. Bloss and H. Schäfer, Rev. Sci. Instrum. **65**, 1541 (1994).
[27] P. Bloss, M. Steffen, H. Schäfer, G.-M. Yang, and G. M. Sessler, IEEE Trans. Dielectr. Electr. Insul. **3**, 182 (1996).
[28] *Landolt-Börnstein*, New Series Vol. III/16a, edited by K.-H. Hellwege (Springer, Berlin, 1981).